Experimental Study of the Grain-Flow, Fluid-Mud Transition in Debris Flows

Jeffrey D. Parsons,[1] *Kelin X. Whipple, and Alessandro Simoni*[2]

Department of Earth, Atmospheric, and Planetary Sciences, Massachusetts Institute of Technology, Cambridge, Massachusetts 02139, U.S.A.
(*e-mail: parsons@ocean.washington.edu*)

ABSTRACT

We have performed a series of laboratory experiments that clarify the nature of the transition between fluid-mud and grain-flow behavior. The surface velocity structure and the speed of the nose of debris flows in channels with semicircular cross sections were measured with several cameras and visual tracers, while the mass flow rate was recorded using a load cell at the exit chamber. Other rheological tests were used to calculate independently the yield strength and matrix viscosity of the debris-flow mixture. Shear rates were varied by nearly an order of magnitude for each mixture by changing the channel radius and slope. Shear rates were significantly higher than expected (6–55 s^{-1}), given the modest slopes examined (10.7°–15.2°). The large values were primarily a result of the concentration of shear into narrow bands between a central nondeforming plug and the sidewall. As a result, the shear rate of interest was calculated by using the width of the shear band and the plug velocity, as opposed to the flow depth and front velocity. The slurries exhibited predominantly fluid-mud behavior with finite yield strength and shear-thinning rheologies in the debris-flow body, while frictional behavior was often observed at the front, or snout. The addition of sand or small amounts of clay tended to make the body of the flows behave in a more Bingham-like fashion (i.e., closer to a linear viscous flow for shear stresses exceeding the yield stress). The addition of sand also tended to accentuate the frictional behavior at the snout. Transition to frictional grain-flow behavior occurred first at the front, for body friction numbers on the order of 100. Similar behavior has been observed in an allied field site in the Italian Alps. In the experiments, it was hypothesized that the snout-grain-flow transition was a result of concentration of the coarsest material at the flow front, reduced shear near the snout, and loss of matrix from the snout to the bed. Regardless of the frictional effects at the snout, flow resistance in the body was nearly always regulated by yield-stress and shear-thinning properties, with no discernible boundary slip, despite volumetric sand contents in excess of 50%.

Introduction

Debris flows, gravity-driven masses of poorly sorted rocks, clay, and organic material, are of fundamental societal importance as a result of the intermittent havoc they produce in mountainous communities throughout the world (Costa 1984). Because of these pressing issues, considerable work has concentrated on the dynamics of these flows. Recent reviews (Coussot and Meunier 1996; Iverson 1997*b*) exhaustively describe the current state of knowledge in this field. Both reviews divide previous debris-flow research into two distinct categories. The first, based upon the pioneering work of Johnson (1965) and Yano and Daido (1965), assumes that debris-flow material behaves as a continuum with an intrinsic yield strength and viscosity. However, these quantities cannot be easily derived from material properties (e.g., grain-size distribution, water content, etc.). Despite this limitation, models based upon the underlying principles of yield-stress fluids have been effective at predicting runout in flows that lack a significant amount of gravel and boulders (Whipple and Dunne 1992; Schwab et al. 1996; Whipple 1997; Huang and García 1999).

The other path of study has been grounded in the mechanics of granular media. Classic research on unimodal grain flows (Bagnold 1954; Savage 1984) has motivated more recent studies that have attempted to alter grain-flow constitutive equations to account for a poorly sorted grain-size distribu-

Manuscript received July 19, 2000; accepted March 5, 2001.

[1] Current address: School of Oceanography, University of Washington, 106 MSB, Seattle, Washington 98195-7940.

[2] Dipartimento di Scienze della Terra e Geo-Ambientali, Università di Bologna, Via Zamboni, 67, 40127 Bologna, Italy.

[The Journal of Geology, 2001, volume 109, p. 427–447] 0022-1376/2001/10904-0002$01.00

tion and/or the presence of pore fluids (Takahashi 1981; Suwa 1988; Iverson 1997*a*, 1997*b*; to name only a few). Grain-flow models, though more grounded in the physics of grain-grain and grain-fluid interactions than the largely phenomenological yield-stress models, are complex and often dependent on parameters not easily estimated without extensive and intrusive measurements (e.g., matrix permeability, pore-water pressure, etc.). Because both of these "models" (and the elegant marriage proposed and advocated by Iverson 1997*b*) are theoretical constructs, they have their advantages and disadvantages. Moreover, rather than simply two distinct models for the same phenomenon, the grain-flow and fluid-mud models are most clearly applicable to distinct types of debris flow. Much experimental data demonstrates that silt-clay slurries are well described by fluid-mud non-Newtonian rheologies (e.g., O'Brien and Julien 1988; Major and Pierson 1992; Coussot and Piau 1995). Conversely, recent experimental studies of fines-poor gravel and sand mixtures have clearly demonstrated that frictional grain-flow models are best applied to these types of flows (e.g., Iverson 1997*b*; Major 1997, 2000). Many natural debris flows have grain-size distributions intermediate between these well-studied cases. Laboratory experiments provide a way to determine the range of applicability of each model. Most interesting to us are the situations that stretch the approximations present in each of these models (e.g., flows where pore fluid rheology is heavily influenced by fines but where sand in the dominant material in the slurry).

As a result, we have attempted to clarify the transition from a friction-dominated grain flow to yield-stress-fluid flow by gradually increasing the silt-clay content of a predominantly sandy slurry. Frictional flows are dominated by grain-grain interactions that are strongly modulated by elevated dynamic pore pressures. Yield-strength flows behave as a fluid-mechanical continuum that can be described by a relatively simple constitutive law (e.g., related to a viscosity and a yield strength, in the case of a Bingham material). Our study has been motivated by an ongoing, comprehensive, observational study in the Italian Alps (Simoni 1998; Berti et al. 1999). The Acquabona debris-flow channel in the Alps exhibits the grain-fluid transition as fine material (silt, extracted from a marl) is eroded from the downstream reach of the channel. The fine material acts to lubricate the flow, increasing runout and initiating what has been interpreted to be yield-strength fluid behavior (Berti et al. 1999).

Rheology of slurries near the frictional fluid transition in sand-dominated debris flows has been explored before (Fairchild 1985; Major and Pierson 1992; Coussot and Piau 1995). However, these studies measured rheological parameters in idealized geometries (i.e., viscometers of varying complexity). Though their data have been useful in obtaining rheologic properties for natural materials, they cannot comment on how shear in free-surface flows distributes itself and how this affects flow resistance and the appearance of the debris flow and its deposit.

Limited work on more natural, free-surface flows also has been performed. These experiments have differed dramatically, depending on the approach. Small-scale devices have typically used predominantly muddy slurries, with little to no sand (Schmeeckle 1992; Coussot 1994), while larger experiments (Iverson and LaHusen 1993; Iverson 1997*a*; Major 1997) have typically used material that lacked a significant silt or clay component. Our experiments and analyses rigorously examine the granular-fluid transition in sandy, but fines-rich slurries (like earlier studies: Major and Pierson 1992; Coussot and Piau 1995) in a more natural, free-surface geometry. Because of the spatial variability of shear rate, we will separately focus on two different portions of the flow: the snout and the quasi-steady body.

Experimental Setup and Procedure

Our experiments were performed in a 10-m long flume in the Experimental Sedimentology and Geomorphology Laboratory at MIT. Each experiment consisted of several runs of the same material, in order to study a single slurry mixture under a variety of conditions (i.e., channel slope and width). The facility (fig. 1) consists of a supply tank (6 m above the laboratory floor) that feeds one of two semicircular channels roughened with a fixed (glued), well-sorted sand (D_{50} = 1 mm). The supply tank has a valve at its base that opens from the top of the tank. The mixture is guided to the appropriate channel by canvas tubing. The channel slope can vary from 10.7° to 15.2°. The slurry was maintained in a well-mixed condition until just before each run with a mixer drill inserted into the tank. (Tests that confirmed homogeneity in the supply tank are discussed in the final section of the analysis.)

Monitoring the flow consisted of two parts. First, surface velocity profiles were obtained with two camcorders at 5 and 8 m down the channel. Black beads that "floated" on the debris-flow surface were

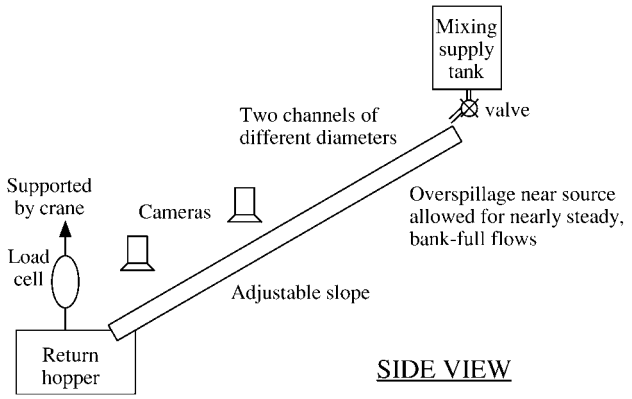

Figure 1. Schematic of the experimental facility

used as tracers. More than 50 beads were laid down along a flow-perpendicular line at a time. Typically, 10 lines were laid down per experimental run, even though run times were often less than a minute long. Lines were chosen for analysis depending on the extent to which the channel was full. Because of the large quantity of material required to fill the 10-m long channel (nearly 500 kg), the flow was only bankfull for the entire length for a few seconds. In the clay-rich experiments, only two lines were observed during bankfull flow. As a result, measurement errors in these experiments (experiments 6 and 7) were large. In all of the other experiments, however, the velocity was well resolved and assessment of error was straightforward, with respect to both precision and accuracy (assumed to be equivalent to repeatability).

Digitized video taken during the experiments allowed for measurement of the displacement of beads between frames (1/30 s for standard video). The distances were measured in pixels, which could be related to length with a photographed ruler using image-processing software. More than 20 velocity measurements could be obtained along the channel cross section with this technique. Errors in precision and repeatability (from one line to the next) were small and reflected in the error estimates of the plug velocity in table 1.

Mass flow rate of the slurry out of the channel was measured using a load cell affixed to a suspended hopper at the base. As the mix poured into the suspended hopper, the weight increased and the analog data from the load cell was transferred to the computer via an A/D board. The A/D board digitized the data at a rate of 4 Hz. Even in the shortest-lived experiments, steady flow was maintained for 2–3 s, making 4 Hz more than sufficient for a mass-flow measurement. Error based on the standard deviation of the mean-flow rate during steady-flow periods is shown along with the mean-flow results in table 1.

Grain-size distributions (fig. 2) in the experiments were based on field studies in the Acquabona channel, an active debris-flow channel in the Italian Alps (Berti et al. 1999). The Acquabona channel has been monitored for several years, and numerous debris flows have been observed during this time (Genevois et al. 1999). Fines are incorporated as the flows run through a marl section. As a result, the flow becomes fines-laden (silt-clay contents in excess of 25%) and exhibits fluid-like behavior (e.g., no slip at the sidewall) while the front remains granular. Describing the rheologic transition in this particular field area was one of the goals of the experiments.

To simulate the extremely wide range (nearly four orders of magnitude) of grain sizes present in our mixtures (fig. 2), material for the experiments came from various sources. Note that the systematic variation in grain-size distribution of the experimental mixtures is achieved primarily by substituting sand for silt. Clay content is held constant at 2.5% by weight of the solids. The fine material (silt and finest sand) used was obtained from U.S. Silica in Ottawa, Ill., while the coarse material was a washed concrete sand (relatively round alluvium) purchased from a local concrete supplier. Clay (kaolinite) was also obtained from the same concrete supplier. Kaolinite is not an active clay (requires less water, binds less strongly, etc.), particularly compared to other common clays (e.g., bentonite). The dominant portion of the material in the finer mixtures, however, consisted of the silts obtained from U.S. Silica. These silts are derived from crushed silica fragments and are highly angular, similar to the landslide material examined by Berti et al. (1999) and Genevois et al. (1999). The debris flows observed by these researchers contained clasts up to meter scale. Only the fraction of material finer than 5 mm was simulated in our experiments. In addition, our experiments involve flow depths about one order of magnitude smaller than typical debris flows. The ramifications of these limitations are elaborated upon in "Discussion."

To obtain homogeneous, well-mixed slurries without sedimentation problems in the mixer, we added water sequentially (usually in 10-kg amounts) to 20–30 kg of fine material (clays first, then silt) mixing thoroughly with a mixer blade attached to a hand drill at each step. Sand was then added incrementally in a large mortar mixer with a small amount of additional water. The full debris mixture

Table 1. Experimental Conditions

Experiment	Material	w	R	Slope (θ)	Snout effect?	U_p	U_{snout}	Q	R_{pp} ($\sim R_{cr}$)
1a	F	16.8	.073	10.7	None	.24 (8.3)	.22 (1.8)	.00189 (1.8)	.0397 (13)
1b			.073	15.2	None	1.17 (10.2)	.87 (1.0)	.00692 (1.3)	.0295 (30)
1c			.05	15.2	Some	.26 (7.8)	.16 (1.7)	.00061 (.4)	.0322 (16)
2a	MF	14.8	.073	10.7	None	.83 (4.8)	.57 (.9)	.00391 (.6)	.0366 (19)
2b			.073	13.7	None	1.69 (2.3)	1.22 (.7)	.00988 (3.7)	.0327 (28)
2c			.05	13.7	Some	.30 (8.3)	.16 (.3)	.00096 (.4)	.0321 (13)
3a	MC	13.8	.073	12.2	Strong	.65 (9.6)	.45 (1.5)	.00448 (1.6)	.0409 (9.1)
3b			.073	15.2	Strong	1.30 (9.0)	1.03 (2.6)	.00888 (5.1)	.0314 (24)
4a	C	13.9	.073	15.2	Strong	.41 (32)	.30 (2.5)	.00275 (15)	.0545 (30)
5a	M	14.2	.073	12.2	Strong	.94 (16)	.61 (.7)	.00554 (1.2)	.0375 (15)
5a2			.073 (wet)	12.2	Strong	1.02 (12)	.77 (.7)	.00649 (3.6)	.0422 (21)
5b			.05	15.2	Strong	.26 (9.0)	.15 (1.4)	.00081 (1.8)	.0343 (18)
5b2			.05 (wet)	15.2	Strong	.27 (9.5)	.22 (6.3)	.00076 (1.0)	.0326 (20)
6a	MC + 2	15.1	.073	12.2	Some	1.02 (25)	1.10 (.8)	.00573 (1.7)	.0401 (6.9)
6b			.073	15.2	Some	1.86 (6.7)	1.19 (.7)	.00963 (1.2)	.0330 (21)
6c			.05	15.2	Strong	.23 (8.0)	.08 (.9)	.00026 (2.1)	.0318 (25)
7a	MC + 3	17	.073	10.7	Some	.91 (15)	.99 (2.0)	.00600 (4.8)	.0371 (25)
7b			.073	15.2	None	2.45 (4.5)	1.79 (1.3)	.01137 (5.9)	.0304 (30)
7c			.05	15.2	Strong	.57 (12)	.36 (2.5)	.00210 (1.4)	.0311 (16)
8a	F	17.6	.073	10.7	Some	.40 (8.7)	.32 (3.6)	.00200 (2.0)	.0396 (18)
8b			.073	12.2	None	.42 (2.8)	.29 (2.7)	.00227 (.3)	.0346 (12)
8c			.073	13.7	None	1.06 (3.3)	.43 (1.8)	.00499 (2.7)	.0302 (33)
8d			.05	13.7	Strong	.16 (1.8)	.10 (.9)	.00031 (1.9)	.0259 (15)
8e			.05	15.2	Strong	.16 (1.9)	.11 (1.9)	.00047 (1.1)	.0238 (23)
9a	CMC	14.4	.05	15.2	Strong, stopped	NA	NA	NA	NA
9b			.05	15.2	Strong, stopped	NA	NA	NA	NA
10	M	13.7	.05, .073	13.7	Strong, stopped	NA	NA	NA	NA

Note. Material abbreviations correspond to the grain-size distributions found in figure 2. The "+" on experiments 6 and 7 indicates the percentage by mass of added clay (in addition to the 2.5% present in all experiments). "Water content" (w) is the percentage of mass of water divided by the total mass of the slurry. "Wet" indicates a thin layer of wet material left on by a previous run (in the pipe radius column). Slope is in degrees. "Stopped" in the snout-effect column means that the flow was arrested before it reached the tailbox (and load-cell). The R_{pp} column is the observed plug radius, which is a close approximation to the actual plug thickness R_c. The subtle difference is discussed in "Analysis." Plug and snout velocities, flow discharges, and plug radii are all in meter-kilogram-seconds, with percentage error in parentheses. Error is representative of both precision and accuracy, which is determined from deviations in multiple measurements. "NA" indicates not applicable or not measured.

was kept well mixed in the mortar mixer until immediately before each experimental run. Though a well-mixed state is not reflective of the initial stages of failure and conversion into a debris flow (Iverson 1997*b*), it is representative of the state of the fluid in distal reaches of debris-flow runout in channels and on fan surfaces where these flows generally present the greatest hazard (e.g., Costa 1984). Moreover, the flows observed by Berti et al. (1999) were in a well-mixed state where the grain-fluid transition occurred.

Experimental Results

Experimental conditions for the flows are shown in table 1; symbols are defined in table 2. All of the slurries had essentially the same density, varying between 2100 and 2300 kg m^{-3}. In all of the experiments, a high-velocity, unsheared core, or plug, occupied a significant portion of the center of the channel, with a rapidly sheared section between it and the sidewall. All flows were laminar. These fluid-like flows appeared to reach a steady state, particularly in the body, within the first few meters of the channel. Steady state flow was verified by the synchronization of multiple cameras and the load-cell measurements. There was also no observable basal or sidewall slip except where frictionally locked snouts formed in experiments with the coarser mixtures and lower boundary shear stresses. Where frictional snouts either did not form or had not formed yet, lack of basal slip caused a conveyor-belt-like flow at the front. Conveyor-belt behavior has been seen previously by other researchers studying subaerial mudflows (e.g., Li et al. 1983; Mohrig et al. 1998). All of these features can be seen from a sequence in figure 3.

In some experiments, frictionally locked snouts

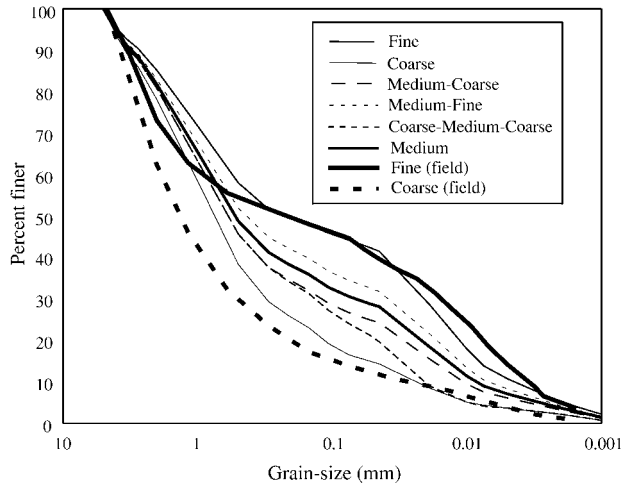

Figure 2. Grain-size distributions of all debris flows studied in the experiments. The field grain-size distributions, with material >5 mm removed, are taken from Berti et al. (1999).

formed and tended to impede flow runout (as seen in boulder- and gravel-rich debris flows in the field: Suwa and Okuda 1983; Whipple 1994; and in large-scale flume experiments: Iverson 1997*b*; Major 1997). These frictional snouts effectively formed dams that moved by basal sliding without internal deformation unless by faulting (fig. 4, last frame). These dams were pushed forward by the pressure of the more fluid and rapidly moving body of the flow, which ponded behind the snout, causing local depths to increase and producing the characteristic bulbous shape of the snout. These frozen snouts would grow from the front backwards as additional material was incorporated into the snout from behind. In some runs this "snout effect" was so pronounced that the snout eventually grew in size to the point that the pressure from behind was insufficient to propel it forward (fig. 4). Beyond this point, any continued discharge of material from the supply tank was forced over the bank. The "snout effect" was so strong with the coarsest mixture (fig. 2) that only in the run in which the slurry was confined in the largest channel on the steepest incline did the flow traverse the length of the flume without being arrested by the snout (experiment 4A; table 1).

It is important to note, however, that in all cases—even those with a pronounced snout effect—the more rapidly sheared body of the flow remained fluid-like with no observable boundary slip. Thus, it appears that our experimental flows varied from macroviscous (no snout effect) to frictional (e.g., Iverson 1997*b*). The onset of frictional behavior appeared to be favored by coarser debris mixtures and lower boundary shear stresses (table 1), qualitatively consistent with the dimensional analysis presented by Iverson (1997*b*). A quantitative assessment of flow regimes and an analysis of the rheology of the rapidly sheared body of the flows are presented in "Discussion."

In addition to the results from the flume experiments, several other tests were performed on the slurry mixtures. Depositional board tests were performed to assess the yield strength of the various slurries. In these tests, a board (roughened in a similar manner to the channels in the flume) was set at three prescribed slopes (at approximately 8°, 10°, and 12°). The expression of Johnson (1970), $\tau_o = \tau_b = \rho g h \sin\theta$, where τ_o is the effective yield stress, τ_b is the basal shear stress, g is the gravitational acceleration, h is the flow depth (in this case, the

Table 2. List of Symbols

Symbol	Definition
D_{50}	Mean grain diameter (L)
err	Subscript that denotes measurement error of a particular quantity (in percent)
g	Gravitational acceleration (L T^{-2})
h	Flow depth (L)
K	Linear coefficient in Herschel-Bulkley model
n	Exponent in Herschel-Bulkley model
N_{BAG}	Bagnold number
N_f	Friction number
N_{SAV}	Savage number
Q	Volumetric flow rate (L^3 T^{-1})
r	Radial direction (L)
ref	Subscript that denotes reference value
R	Channel radius (L)
R_{cr}	Nondeforming plug radius (L)
R_{pp}	Apparent plug, or pseudoplug, thickness (L)
T_{err}	Total average error used in minimization routine
U	Streamwise velocity
U_p	Plug velocity (L/T)
$URMS_x$	Root-mean-square uncertainty calculated in the parameter x
v_s	Volumetric solids concentration
δ	Grain diameter in dimensionless number calculations (L)
γ	Shear rate (1/T)
μ	Matrix viscosity (ML^{-1} T^{-1})
θ	Channel slope, in degrees
ρ	Overall density, 2100–2300 kg/m^3
ρ_s	Density of solids, 2650 kg/m^3
ρ_f	Density of interstitial fluid (estimated from fines content and bulk density)
τ_o	Yield strength (ML^{-1} T^{-2})
τ_b	Bed shear stress (ML^{-1} T^{-2})
τ_{rx}	Shear stress acting in the down-channel direction

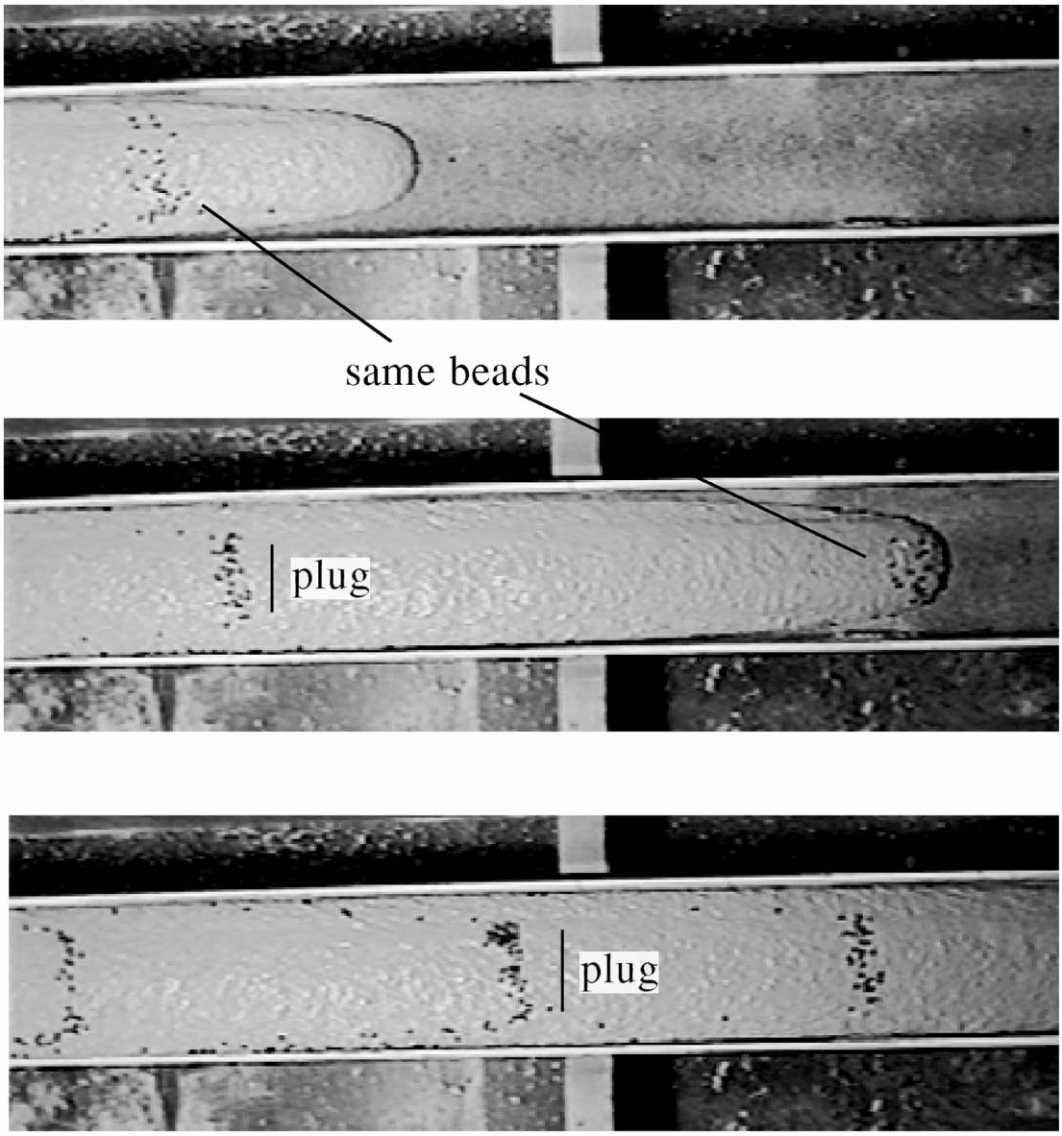

Figure 3. Sequence of frames illustrating smooth, well-behaved debris flow. The first two frames indicate the "conveyor belt" of material circulating at the front (i.e., the tracers traveling to the snout are subsequently buried). Later frames illustrate the no-slip behavior at the sidewalls and the significant plug in the center of the channel. The frames shown were taken approximately 1 s apart during experiment 2 (for experimental conditions, see table 1). The pipe shown is 0.075 m in radius.

thickness of a rapidly formed deposit), and θ is the bed slope, was used to estimate the effective yield stress of each mix. After the slurry was poured quickly out over most of the board, the deposit froze en masse, and the depth was measured in several locations (two to four) with a ruler (accuracy, 1 mm). The deposits on the depositional board were thin, tabular, and lobate, as expected for a viscoplastic material. Thickness variations were generally less than 10% away from the periphery of the deposit. More significantly, average deposit thickness was found to be inversely proportional to $\sin\theta$ ($R^2 \geq 0.96$ in all cases), such that estimated yield strengths were constant (<10% variation from the mean) over the range of slopes used. This finding implies that the constant yield strength model is both relevant and accurate. Mean values and 1σ errors (%) are given in table 3. Estimated yield strengths also varied in a consistent manner, rising as the mix became coarser.

Viscosities of the "matrix" component of the debris mixtures were measured with a Brookfield

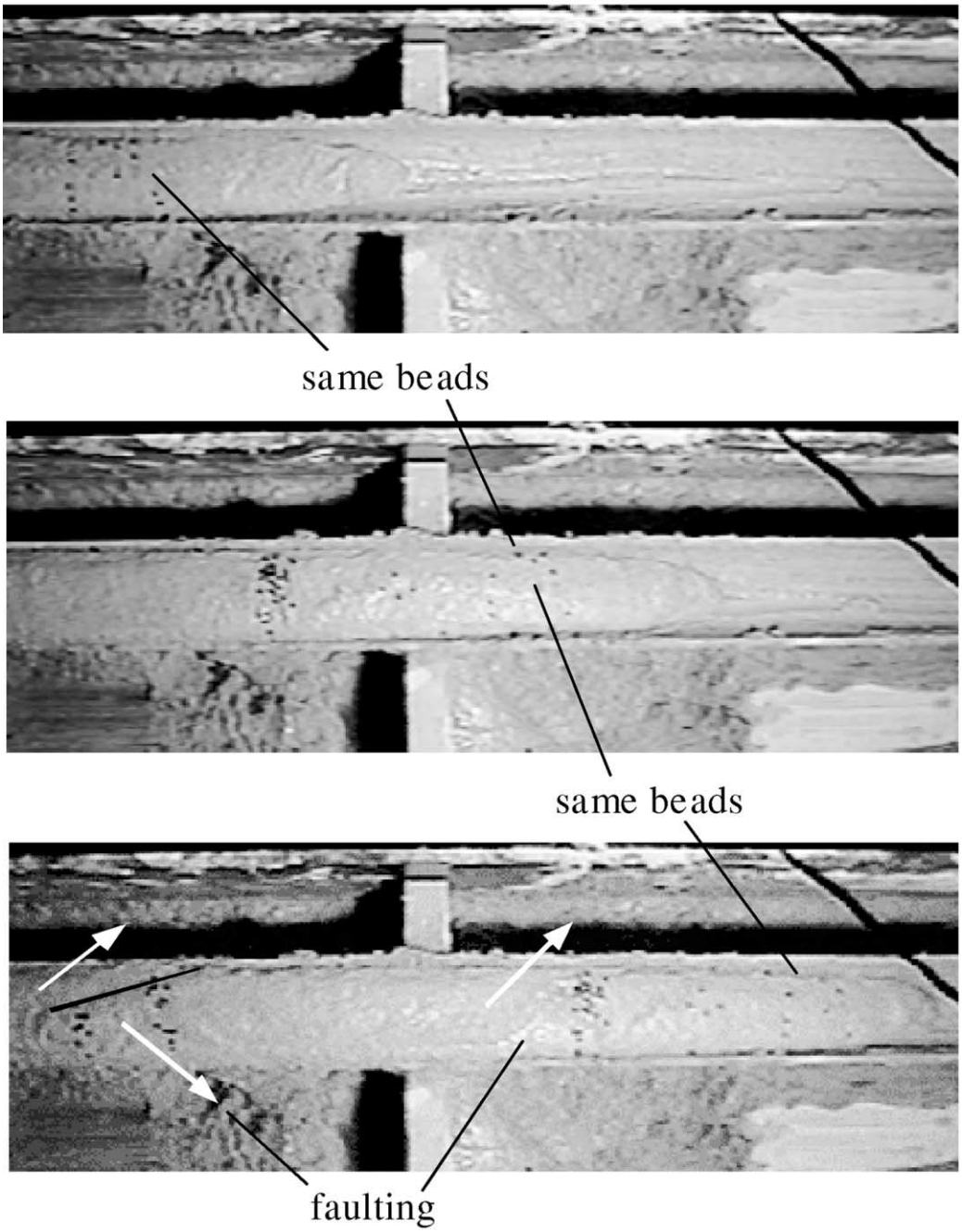

Figure 4. Sequence of frames illustrating arresting snout (experiment 4C). Time between the first frame and the second is approximately 3 s, while the third frame is 15 s after the second. The pipe shown is the small pipe (0.05 m in radius).

Model LVF Dial Viscometer (an adjustable, cylindrical viscometer). We assumed that the matrix consisted of all of the material that was silt and clay sized (i.e., $D < 63$ μm). We also assumed that it contained all of the water that was present in the bulk mix. Because some water will bind to sand grains, our matrix viscosity estimates will be conservative lower bounds. A range of water contents was examined for each matrix. Note that, because the percentage of clay in the total mixture was held constant, the relative abundance of clay in the matrix varies systematically, becoming greater in the

Table 3. Results of the Tilting Board and Viscometer Tests

Experiment (mix)	τ_o (Pa)	r^2	μ_{matrix} (Pa-s)
1 (fine)	54 (4)	.99	1.2
2 (medium fine)	55 (3)	.98	.9
3 (medium coarse)	98 (2)	1	.4
4 (coarse)	113 (2)	.97	.06
5 (medium)	67 (5)	.99	.4
6 (medium coarse + 2% clay)	121 (3)	.97	.5
7 (medium coarse + 3% clay)	73 (8)	.96	.4

Note. The r^2 values for the yield strength are those for the linear relationship of Johnson (1970), $\tau_o = \tau_b = \rho g h \sin\theta$, where τ_o is the effective yield stress, τ_b is the basal shear stress, g is the gravitational acceleration, h is the flow depth (in this case, the thickness of a rapidly-formed deposit), and θ is the bed slope. Matrix viscosity measurements are reflective of interpolations between values measured separately. The 1σ variations of yield strengths in parentheses are in Pa. Error in matrix viscosity measurements is high and can be considered roughly one order of magnitude. Units are all meter-kilogram-seconds.

coarser mixtures. For each matrix composition, as the water content was increased, measured viscosities decreased exponentially. This observation is consistent with many previous studies (fig. 5). Because the water content of the total mix could not be prescribed exactly beforehand, the values in table 3 were interpolated from the data in figure 5. The only exception was for the coarsest mix (experiment 4), where nearly all of the material was sand. In this case, the viscosity had to be extrapolated because of the very dilute nature of the matrix in the coarse debris slurry. However, the assumption that none of the water was bound to sand grains is probably poor.

As can be seen in figure 5, our matrix viscosity estimates are in good agreement with other studies. In all cases, except the study by Schmeeckle (1992), decreasing clay contents are characterized by (1) lower viscosities for a given water content and (2) an increased sensitivity to water content (i.e., the slope of the lines on the semilog plot steepen with lower clay contents). In both these respects, our matrix slurries are intermediate between the relatively clay-rich slurries of O'Brien and Julien (1988) and the clay-poor slurries of Major and Pierson (1992). The more clay-rich matrix of the coarse mixture approximates the 5%–7% clay data of O'Brien and Julien (1988). Similarly, the matrix of the fine mixture is approaching the relation given by Major and Pierson (1992) for their clay-poor, fines-only sample (<63 μm; fig. 5). This degree of concurrence gives us confidence in the viscosity estimates obtained with the Brookfield viscometer. As a matter of speculation, the well-sorted, very fine-grained nature of the silts used by Schmeeckle (1992), which included a considerable fraction of angular, clay-sized (~1 μm) silica fragments, may explain the unusual low sensitivity to water content in this clay-mineral-free material. Finally, it is notable that the empirical relation given by Thomas (1965) for suspensions of uniform spherical particles grossly underpredicts the viscosity (2–3 orders of magnitude) of slurries of poorly sorted and angular natural debris. The underprediction is greatest for slurries containing even small amounts of clay.

Analysis

Dimensional Analysis of Flow Regime. There are three sources of impedance to motion in these flows: collisional, frictional, and viscous. Depending on the strength of each of these forces, the flow will evolve differently. Iverson (1997*b*) formulated and summarized the three dimensionless variables that describe the relationship between these three effects. He also presented preliminary constraints on the magnitudes at which these dimensionless parameters transition from one force being dominant over the other. The mathematical expressions

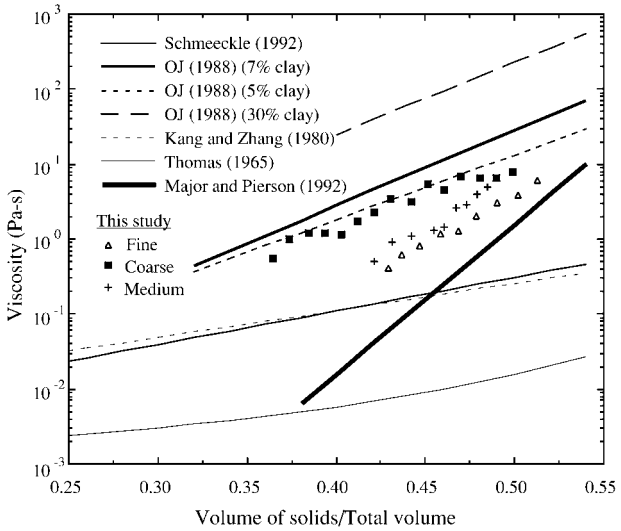

Figure 5. Comparison of various empirical relationships with the data obtained in this study. "OJ (1988)" refers to O'Brien and Julien (1988). The Major and Pierson (1992) relationship is for their material <63 μm (i.e., silt and clay only). Thomas (1965) is the relationship used by Iverson (1997*b*), and Kang and Zhang (1980) represents the relationship for a poorly sorted silt.

describing each of these parameters are (Iverson 1997*b*) the Bagnold number (the ratio of collisional to viscous forces)

$$N_{\mathrm{BAG}} = \frac{v_s \rho_s \delta^2 \gamma}{(1 - v_s)\mu}, \tag{1a}$$

the Savage number (the ratio of collisional to frictional forces

$$N_{\mathrm{SAV}} = \frac{\rho_s \delta^2 \gamma^2}{(\rho_s - \rho_f) g h \tan \phi}, \tag{1b}$$

and the friction number (the ratio of frictional to viscous forces)

$$N_f = \frac{v_s (\rho_s - \rho_f) g h \tan \phi}{(1 - v_s)\gamma \mu}, \tag{1c}$$

where γ denotes the shear rate, ρ_s the clast density (2.6 kg m^{-3} for quartz, the material used), ρ_f the estimated interstitial fluid density, δ the mean grain size (table 1), v_s the mean volume fraction of solids (related to the water content via the submerged specific gravity of the clasts; see table 1), μ the viscosity of the interstitial fluid (table 3), h the flow depth (table 1), ϕ the angle of internal friction (assumed to be 42°; Simoni 1998), and g the gravitational acceleration (9.81 m s^{-1}). According to available experimental constraints (albeit largely restricted to experiments with unimodal spherical particles), collisional forces dominate over viscous forces for $N_{\mathrm{BAG}} > 200$, collisional forces dominate over frictional forces for $N_{\mathrm{SAV}} > 0.1$, and frictional forces dominate over viscous forces for $N_f > 2000$ (Bagnold 1954; Savage and Hutter 1989; Iverson 1997*b*).

Following Iverson (1997*b*), the interstitial fluid density was estimated by assuming the entire mass of silt and clay (and no sand) contributed to the interstitial fluid. That is, if the sand content was 100%, the interstitial fluid density would be the density of water, while if there were no sand and only fines, the interstitial fluid density would be equal to the bulk density.

All of these quantities were either measured or estimated directly. The only exception is the shear rate γ, which has to be calculated. Assessments of natural debris flows typically estimate γ by dividing the snout or plug velocity by the flow depth (e.g., Phillips and Davies 1991; Iverson 1997*b*). Previous rheological work (Major and Pierson 1992; Coussot and Piau 1995) has constrained the value of γ through the use of constructed geometries. Because of the direct flow visualization in our experiments, we were able to use the shear rate definition that regulates runout in a free-surface flow. From our observations, the relevant shear rate is defined by the ratio of the plug velocity and the shear width (the distance between the plug and the sidewall). Because the plug does not participate in the shearing process, it should not be included in the calculation. The shear width was defined by the distance to the sidewall where the measured velocity profile was "indistinguishable" from the plug speed. In the next section, the difference between this "pseudoplug" and an actual rheological plug (i.e., where shear stress is less than the material yield strength) will be discussed at length. A comparison was made (table 4) of these two different methods for obtaining the shear rate, along with the calculations of the various dimensionless parameters. The value we propose presents considerably larger values of the shear rate than the traditional method. Flow depth and snout velocity are, however, probably more representative of the conditions at the snout, where the entire cross section is deformed and the fluid velocities are smaller.

Regardless of definition of the shear rate, dimensional analysis using the critical Bagnold, Savage, and friction numbers places our flows either in the viscous regime or near the transition from viscous to frictional regimes (table 4). Body friction numbers (N_{f1}) predict viscous behavior for all except the coarsest mixture (experiment 4), which has a friction number near the threshold value. Snout friction numbers (N_{f2}) predict important frictional effects for the medium, medium-coarse, and coarse debris mixtures, at least in configurations with lower boundary shear stresses (gentler flume slopes and smaller channel radii). For the coarsest mixture—which failed to traverse the length of the flume except when run down the larger channel set at the steepest inclination (experiment 4A)—the snout friction number is well into the frictional range. Contrary to the speculations of Iverson (1997*b*) about the grain-size characteristics of flows likely to exhibit macroviscous behavior, most of our flows were predominantly sandy with low water contents. We believe there are our two causes for the deviation from previous analyses. First, the interstitial viscosities of our slurries (table 3) are considerably higher than some previous estimates (Thomas 1965; Schmeeckle 1992) but not all (O'Brien and Julien 1988; fig. 5). The high viscosities are most likely a result of the poorly sorted, highly angular makeup of the constituent silts and the presence of a minor but nonnegligible amount of clay. Second, the relevant shear rates in our free-surface flows were considerably higher than the 1–5

s^{-1} range that has been argued by some to be relevant to debris-flow runout in channels and on fan surfaces (O'Brien and Julien 1988; Phillips and Davies 1991; Major and Pierson 1992).

Rheology of the Debris-Flow Snout. As described qualitatively earlier, frictional effects were observed at the front or snout of many of the experimental flows. Because of the increased friction number there (N_{f2}, defined by the snout velocity and flow depth at the snout) and other sorting effects to be discussed below, the flow transformed from fluid to frictional behavior from the snout backward. This flow transition could be seen qualitatively in "strong-snout-effect" runs (seen in table 1) as a freezing or interlocking in a large region near the snout (that moves by basal sliding), while some runs simply appeared to be slowed near the snout and the conveyor belt action near the front was reduced ("some snout effect"). In the most fluid-like flows ("no snout effect"; table 1), no frictional effects were observed anywhere.

Dividing the runs into these three categories, a critical friction number can be postulated. All but one of the strong-snout-effect runs have body friction numbers in excess of 130, and all but two have snout friction numbers above 400. Neither body nor snout friction numbers of the no-snout-effect and some-snout-effect runs are statistically separable. However, the onset of some frictional behavior appears to occur at body friction numbers of ~100 and snout friction numbers of ~250 (table 4). The threshold value (~100) is considerably lower than the value (~2000) obtained by Iverson (1997*b*) from a combination of more idealized experiments (Bagnold 1954; Savage and Hutter 1989). Although the large error in the matrix viscosity estimate (conservatively up to an order of magnitude, despite our agreement with previously published estimates; fig. 5) makes definitive calculations of a transition friction number impossible, the transition friction number does appear (within experimental error) to be significantly smaller than the previously accepted estimate. Perhaps more important is the observation that the transition to frictional behavior appears to be restricted to the slowly deforming snout region and occurs in flows that otherwise behave in a macroviscous manner. Thus, for many transitional flows the relative importance of fluid rheology and the frictional behavior of the snout may be difficult to assess.

Table 4. Comparison of Different Shear Rate Definitions and Their Resulting Friction Numbers

Experiment run	γ_1	γ_2	N_{f1}	N_{f2}	N_{BAG}	N_{SAV}
1A	6.8	2.9	164	380	.002	7.1E-06
1B	25.7	11.6	43	96	.007	1.0E-04
1C	14.6	3.2	51	232	.004	4.9E-05
2A	21.6	7.6	89	253	.028	2.3E-04
2B	40.0	16.3	48	118	.052	7.9E-04
2C	16.8	3.2	76	401	.022	2.1E-04
3A	19.1	6.0	271	862	.107	3.2E-04
3B	29.8	13.7	173	377	.168	7.9E-04
4A	20.0	4.0	1868	9338	1.672	7.9E-04
5A	25.1	8.1	190	587	.095	3.9E-04
5A2	31.1	10.3	153	465	.117	5.9E-04
5B	16.6	3.0	192	1061	.063	2.5E-04
5B2	15.5	4.4	205	723	.059	2.2E-04
6A	29.2	14.7	127	254	.118	7.5E-04
6B	44.3	15.9	84	235	.179	1.7E-03
6C	12.6	1.6	196	1552	.051	2.1E-04
7A	24.0	13.2	168	306	.106	5.1E-04
7B	54.9	23.9	74	169	.241	2.7E-03
7C	30.2	7.2	89	374	.133	1.2E-03
8A	11.3	4.3	118	312	.003	2.0E-05
8B	10.4	3.9	128	344	.003	1.7E-05
8C	23.7	5.7	56	232	.007	8.6E-05
8D	6.6	2.0	134	444	.002	1.0E-05
8E	6.1	2.2	145	403	.002	8.6E-06

Note. Indices indicate the two different shear definitions discussed in the text. They are (1) traditional estimate: snout velocity and flow depth, (2) proposed value: plug velocity and shear width. Savage and Bagnold numbers are calculated with the shear rate defined by the shear width and plug velocity. Only experiments where flow discharge was obtained are shown (i.e., snout-stopping flows were not included).

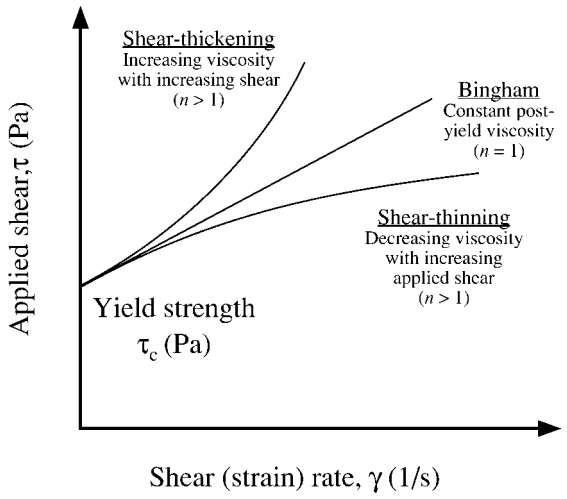

Figure 6. Diagram illustrating Bingham, shear-thinning, and shear-thickening behavior.

Rheology of the Quasi-Steady Debris-Flow Body. Because of the no-slip behavior at the sidewall and the particular combination of dimensionless parameters in our flows, it was readily apparent that the bodies of the flows, particularly in the shearing region, were predominantly fluid-like. Considerable work has concentrated on the rheology of fluids that have a significant sand component. Early stud-

ies (O'Brien and Julien 1988; Phillips and Davies 1991) demonstrated the strong dependence of fines (silt-clay) content and water content. They also demonstrated that rheology was strongly dependent on shear rate and postulated that low shear rates ($\gamma < 10\ s^{-1}$) were most relevant to natural debris flows. In later work, Coussot and Piau (1995) used a field rheometer on Alpine debris-flow materials, quite similar to those simulated here, to examine the utility of the Herschel-Bulkley model. The Herschel-Bulkley model is a generalized formulation of continuum behavior in a yield-stress fluid. Figure 6 illustrates the difference between the various models discussed. Coussot and Piau (1995) found that their samples, sieved at 2 cm, possessed relatively high yield strengths (100–400 Pa) and exhibited strongly shear-thinning behavior (n = 0.15–0.35). In other experiments, Major and Pierson (1992) found shear-thinning behavior (n = 0.3–0.9) for silt/clay-dominated slurries and Bingham behavior (approximately $n = 1$) for highly sheared ($\gamma > 5\ s^{-1}$) sandy slurries.

Following earlier work (Major and Pierson 1992; Coussot and Piau 1995), we characterized our flows using the general Herschel-Bulkley model. The derivation of characteristics (plug velocity, etc.) for Herschel-Bulkley fluids in semicircular channels has been presented before (e.g., appendix in Mohrig et al. 1999). However, Mohrig et al. (1999) did not exploit the analysis for the assessment of postyield properties but only for an estimation of the yield strength. The applicability of a constant yield-strength model to the experimental slurries was demonstrated by the tilting board analysis (table 3). It will be independently verified below.

We begin with the general Herschel-Bulkley model for non-Newtonian fluids in steady, uniform open channel flow of semicircular cross section:

$$\tau_x - \tau_o = K\left(\frac{du}{dr}\right)^n; \quad \tau_x \geq \tau_o, \tag{2a}$$

$$\tau_x = \frac{1}{2}\rho g r \sin\theta, \tag{2b}$$

where τ_x denotes shear stress acting in the downchannel direction (x), τ_o is the yield stress, K is a linear coefficient, which for Bingham behavior ($n = 1$) corresponds to a viscosity, u is the downstream velocity, r is the radial direction ($r = 0$ at the channel axis and $r = R$ at the wall), ρ is the bulk density, g is the gravitational acceleration, θ is the channel slope, and n is a positive constant. A nondeforming plug region forms wherever $\tau_x \leq \tau_o$ (or $r \leq R_{cr}$) (Johnson 1965). The variable R_{cr} is defined by

$$R_{cr} = \frac{2\tau_o}{\rho g \sin\theta}. \tag{3}$$

Using equations (2b) and (3), a nondimensional plug radius may be written

$$\frac{R_{cr}}{R} = \frac{\tau_o}{\tau_b}, \tag{4}$$

where τ_b is the boundary shear stress (at $r = R$). Integrating equations (2) once and applying a no-slip boundary condition gives relations for the steady, uniform, radial velocity profile,

$$U(r) = \frac{(\tau_b/K)^{1/n}R}{1 + 1/n} \times [(1 - \tau_o/\tau_b)^{1+1/n} - (r/R - \tau_o/\tau_b)^{1+1/n}], \tag{5a}$$

$$U_p = \frac{(\tau_b/K)^{1/n}R}{1 + 1/n}(1 = \tau_o/\tau_b)^{1+1/n}, \tag{5b}$$

where U_p is the plug velocity. Integrating equation (5) in r and around the arc of the semicircular channel section gives a relation for flow discharge (Q):

$$Q = \frac{(\tau_b/K)^{1/n}\pi R^3}{1 + 1/n} \times \left[\frac{(1 - \tau_o/\tau_b)^{1+1/n}}{2} - \frac{(1 - \tau_o/\tau_b)^{2+1/n}}{2 + 1/n} + \frac{(1 - \tau/\tau)^{3+1/n}}{(2 + 1/n)(3 + 1/n)}\right]. \tag{6}$$

Thus, the problem involves three equations ([4], [5b], [6]) and three unknown rheological properties (τ_o, K, n). Nondeforming plug radius R_{cr}, plug velocity U_p, and flow discharge Q of our experiments can be found with error estimates in table 1. It is possible to calculate all of these rheological properties with entirely nonintrusive measurements. Because of the remote nature of the measurements, the analysis herein could be extended to in situ rheological examination of field-scale flows, if the proper location was chosen (i.e., a muddy, laminar flow in a nearly semicircular channel).

A comparison of flow discharge (measured at the flume exit) and surface velocity data affords a preliminary test of the hypothesis that the quasi-steady stage of the experimental flows (i.e., well

behind the frictional snout for transitional flows) could be well described as homogeneous fluids with non-Newtonian rheology. The velocity field of a laminar, homogeneous fluid in a channel with a semicircular cross section is expected to be axisymmetric (e.g., Johnson 1965; eqq. [2]–[6]). Frictional grain flows by comparison will not exhibit axisymmetric velocity fields because of the increased normal forces in the deepest part of the channel. Thus, a radial integration of the surface velocity profile should match measured discharges if and only if the material is behaving as a homogeneous fluid. In all experiments, integration of the velocity reproduced the independently measured flow discharge within the accumulated error of the surface velocity measurements (i.e., 20%). Although this provides some measure of support to the application of a homogeneous-fluid rheology, the test is not a strong one; at the limited depths and rapid shear rates of our experimental flows the deviation from axisymmetry in frictional grain flows may not be large. A more convincing test is whether constant values of (τ_o, K, n) can be found that explain all the experimental data over the full range of flow conditions tested, including the tilting board tests for material yield strength.

We begin by testing the validity of the constant yield strength assumption based on observed plug thickness as a function of imposed basal shear stress. The test is critically important because, as Iverson (1997*b*) and others have pointed out, the existence of a nondeforming plug does not necessarily imply the existence of a finite yield strength; any number of granular flow models without a plastic yield strength predict nondeforming plugs in the right circumstances. Equation (4) can be rewritten in a nondimensional form that allows us to test this assumption directly. Normalizing both sides of equation (4) by a reference value gives the relation

$$\frac{R_{\mathrm{cr}}/R}{(R_{\mathrm{cr}}/R)_{\mathrm{ref}}} = \frac{\tau_o/\tau_b}{(\tau_o/\tau_b)_{\mathrm{ref}}} = \frac{\tau_{b_{\mathrm{ref}}}}{\tau_b}, \qquad (7)$$

where the second equals sign is true if and only if the yield strength is constant over the range of flow conditions tested. Equation (7) predicts normalized plug thickness to decrease monotonically with increasing normalized boundary shear stress. For all runs in a given experiment (e.g., experiment 8A–8E), we take the reference value to be that measured for the run with the lowest boundary shear stress (e.g., experiment 8A). The normalized plug thickness data for all runs collapses to a single curve that is well predicted by equation (7) (fig. 7). Granular flows are expected to have the opposite behavior, because it is the shear band width that is expected to remain constant with channel radius for granular flows (Savage 1984; Haff 1986). This implies that normalized plug thickness would increase rapidly with channel radius, as illustrated schematically on figure 7. As can be seen in the figure, all but one of the runs agree with a constant yield strength model within experimental error. Although our discussion of expected plug thickness variations for a granular material is highly simplified, there is no experimental basis to reject the constant yield strength assumption.

Most significant to our analysis was the determination of the postyield properties (K, n). Because equations (4), (5b), and (6) could be solved for (τ_o, K, n) for each experimental run, the properties of each mix were overdetermined (as the result of the three to five runs per mixture). The solution of the equations is therefore a minimization problem. To find best-fit combinations of rheological parameters, we seek to minimize the residuals between measured and estimated values of the measured variables (R_{cr}, U_p, Q) for each experiment. Estimated values of R_{cr}, U_{p}, Q were computed from equations (4), (5b), and (6), respectively.

The root-mean-square residual error for each measured quantity (URMS_Q, $\mathrm{URMS}_{U_{\mathrm{p}}}$, $\mathrm{URMS}_{R_{\mathrm{cr}}}$) for each run in a given experiment was calculated for a wide range of realistic parameter values (i.e.,

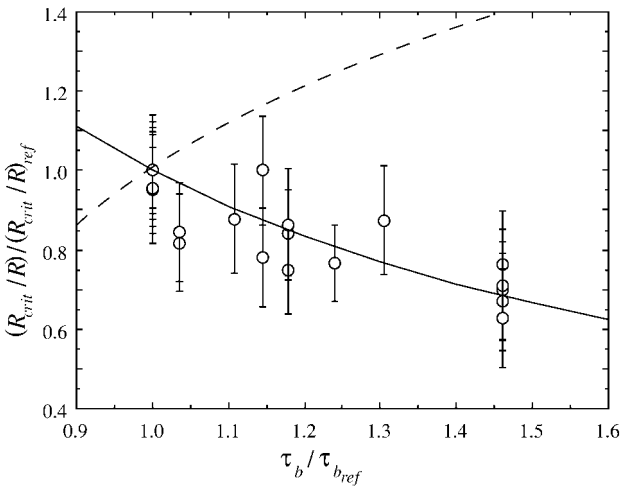

Figure 7. Relationship between relative bed shear stress and relative plug thickness for each mix examined (along with experimental error bars). Solid line represents that expected for constant yield strength behavior (eq. [4]). The dashed line is reflective of the general trend expected from a frictionally dominated flow.

$1 < \tau_o < 200$, $0.1 < n < 2$, $0.1 < K < 50$). Because measurement error varied greatly depending on the quantity examined, the residual errors were weighted accordingly in the minimization scheme. The weighting was done in a linear manner, according to

$$T_{\text{err}} = \frac{\text{URMS}_Q/R_{\text{cr}_{\text{err}}} + \text{URMS}_{U_p}/R_{\text{cr}_{\text{err}}} + \text{URMS}_{R_{\text{cr}}}}{Q/R_{\text{cr}_{\text{err}}} + U_{p_{\text{err}}}/R_{\text{cr}_{\text{err}}} + 1}, \quad (8)$$

where URMS_Q, URMS_{U_p}, $\text{URMS}_{R_{\text{cr}}}$ are the residual errors of the worst run in each experiment for each quantity. The total error T_{err} is the parameter that was ultimately minimized in the search routine.

The analysis is complicated somewhat because the measurement error in the plug thickness R_{cr} is also a function of n. As $n \to 0$, the apparent plug thickness R_{pp} will be an increasingly poor estimate of the actual plug thickness because low rates of deformation expected in the interior of the flow for shear-thinning materials cannot be resolved within the error in our velocity measurements. These slowly deforming areas outside the rheologic plug would therefore be included in the observed "pseudoplug" radius R_{pp}. Figure 8 illustrates this effect along with the definition of the pseudoplug for a velocity profile obtained from experiment 1C. The pseudoplug thickness is the actual parameter measured and reported in table 1. However, we can estimate the error in R_{cr}, in terms of the error in the velocity measurements (the U_p error in table 1 is reflective of both precision and repeatability). The difference between the pseudoplug thickness R_{pp} and the rheologic plug thickness R_{cr} depends directly on the velocity measurement error. The measured pseudoplug will extend to the point that the difference between local flow velocity $U(R_{\text{pp}})$ and the plug velocity U_p is equal to or greater than the measurement error U_{err}, which is defined as

$$U_{\text{err}} = \frac{U_p - U(R_{\text{pp}})}{U_p}. \quad (9)$$

Similarly, the pseudoplug thickness error is defined as $R_{\text{pperrcalc}} = (R_{\text{pp}} - R_{\text{cr}})/R_{\text{cr}}$. Substituting equations (5a) and (5b) for $U(R_{\text{pp}})$ and U_p in equation (9), respectively, and solving for $R_{\text{pperrcalc}}$ yields an expression for the pseudoplug error in terms of n and the velocity measurement error U_{err}:

$$R_{\text{pperrcalc}} = \left(\frac{R}{R_{\text{cr}}} - 1\right) U_{\text{err}}^{n/(1+n)}. \quad (10)$$

Only for strong shear-thinning rheologies ($n < 0.5$) will $R_{\text{pperrcalc}}$ be large. Because error in the original measurement of R_{pp} is significant (typically 10%–20%), only in experiments 1 and 5 were the errors due to the "pseudoplug effect" larger than the initial measurement error (table 1). In these two cases, we replaced the error calculated from equation (10) in our minimization scheme for the measured error in R_{pp} reported in table 1.

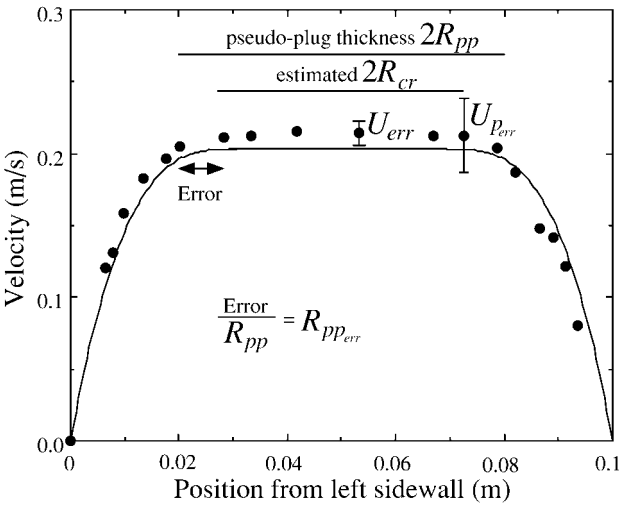

Figure 8. Velocity profile obtained from experiment 1C illustrating pseudoplug, estimated plug thickness, and the errors associated with measurement. Solid circles represent individually measured velocities, while the line was obtained from equation (5a), using the rheological parameters in table 5. The results shown are typical of all of the clay-poor experiments. The estimated R_{cr} was obtained from the minimization analysis and is also approximately the lower bound of R_{cr} examined in equations (8)–(10).

Using the method above, the in situ rheological parameters were calculated along with an estimation of their uncertainty (table 4). The Herschel-Bulkley model was found to perform well. Plug velocities, flow discharges, and plug thicknesses predicted with best-fit Herschel-Bulkley parameters satisfactorily explain all experimental data (fig. 9). Trends in the estimated rheological parameters as a function of grain-size distribution, in both external (tilting-board) and in situ (flume experiments), were quite evident. In both the tilting-board measurements and the in situ calculations, yield strengths increased with increasing coarse material and clay content. The yield strength estimates derived by these independent methods also agree remarkably well (fig. 10). In situ rheological parameters indicated other trends as well. For instance, shear thinning became increasingly domi-

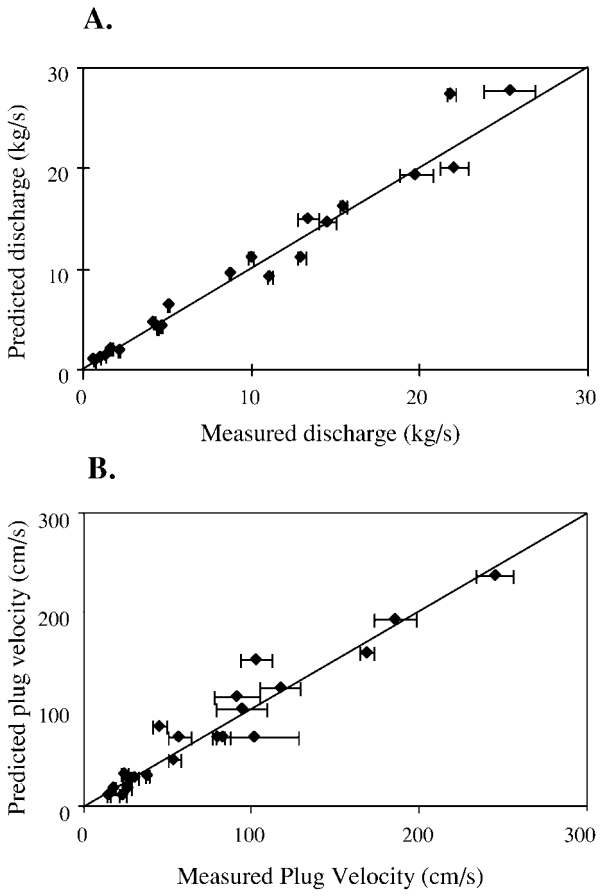

Figure 9. Evaluation of the performance of the Herschel-Bulkley model. *a*, Comparison of calculated discharges (eq. [6]) using best-fit rheological parameters (table 5) to measured values (table 1). *b*, Comparison of the calculated plug velocities (eq. [5b]), using the best-fit rheological parameters (table 5) to measured values (table 1).

nant as the mixes became fines-dominated, while the addition of extremely small amounts (1%–3%) of clay made the flows nearly Bingham. All of these qualitative trends were observed by earlier rheometric work, though our flows were generally less shear thinning. The reduction in shear-thinning behavior (particularly as compared to Coussot and Piau 1995) was possibly a result of the high sand contents in our experimental slurries, consistent with the data and analysis of sand-rich slurries presented by Major and Pierson (1992).

For the purpose of comparison, the minimization routine was also adapted to assess the performance of the Bingham ($n = 1$) model, by simply removing n as a free variable. The Bingham assumption is common in many modeling applications (e.g., Whipple 1997; Huang and García 1999), and it is useful to quantify the error incurred by its application to our experimental flows. This analysis has the side benefit of providing best-fit estimates of a Bingham viscosity for the bulk debris mixtures for comparison to matrix viscosity estimates. The results in table 6 demonstrate that, aside from the clayey experiments, viscosities were in excess of 1 Pa-s. These viscosities are surprisingly close to (given the high sand contents), but somewhat larger than, the matrix viscosity measurements (table 3). As explained below, a systematic overestimate of yield strength in the case of the Bingham fits resulted in an artificial reduction in the best-fit Bingham viscosities. Nonetheless, some combination of loss of water from the matrix slurry to adhesion to fine sand particles and participation of some fraction of the sandy component in the bulk viscosity are probably responsible for the greater viscosity of the bulk mixtures.

Though the Bingham model did not perform as well as the more general Herschel-Bulkley model (compare residual errors in tables 5, 6), the errors were not significantly larger. The largest deviations in the Bingham model appear to be in the assessment of the yield strength. The least-squares routine favored the discharge and plug velocity data (the most accurate measurements) and passed most of the miss-fit of the Bingham model to the assessment of the yield strength (tables 5, 6). As a result, the tilting-board tests of yield strength agreed well with Herschel-Bulkley calculations but not with the Bingham numbers. The exaggerated

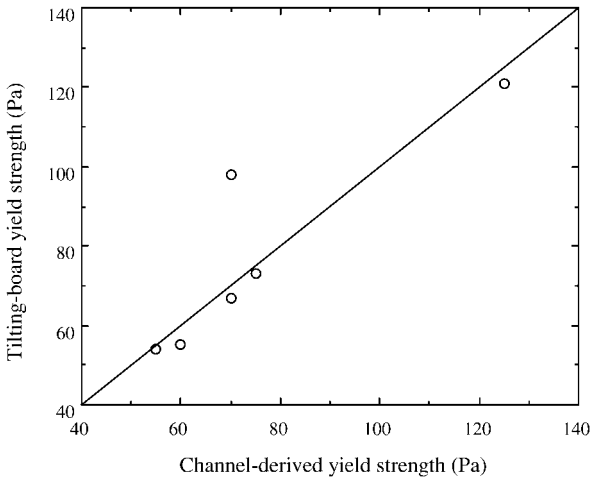

Figure 10. Comparison of the tilting-board yield strengths (table 3) with the channelized values obtained from the Heschel-Bulkley minimization routine (table 4).

Table 5. Yield-strength rheologic parameters for the non-snout-stopped experiments

Experiment (mix)	τ_o (Pa)	K (Pa-s)$^{1/n}$	n	URMS$_{R_{cr}}$	URMS$_{U_p}$	URMS$_Q$
1 (fine)	55	22.5	.45	3.7	6.6	.5
2 (medium-fine)	60	8.8	.60	1.7	.4	1.1
3 (medium-coarse)	70	7.1	.70	4.2	1.1	.8
5 (medium)	70	15.8	.43	3.2	.3	.5
6 (medium-coarse + 2% added clay)	125	.5	1.08	23	22	3.4
7 (medium-coarse + 3% added clay)	75	.5	1.25	1.0	1.8	.7
8 (fine)	43	31	.43	2.5	2.0	2.5

Note. Uncertainties (in percent) are the root-mean-square differences between the calculated and observed parameters (R_{cr}, U_p, Q) using the selected parameter set (τ_o, K, n) in equations (4), (5b), and (6).

yield strengths also caused the calculated in situ viscosities to be artificially low, masking the participation of sand in the viscosity. Regardless, the errors were small (only slightly greater than measurement error) and will only be important if the rheological parameters are used over a large (greater than an order of magnitude) range of the basal shear stress.

In summary, all of the experimental data obtained from the quasi steady flow away from the influence of any frictional snout are consistent with a non-Newtonian fluid rheology, similar to the results of Coussot and Piau (1995) and Major and Pierson (1992) (for $\gamma > 5$ s^{-1}). Again, this is not surprising considering the friction numbers examined, given our estimates of matrix viscosity. Although we have not evaluated whether the frictional debris-flow model due to Iverson (1997*b*) could be modified to explain our experimental data (by accounting for the high viscosity and finite strength of the interstitial fluid), the best interpretation, given available data, is that our experimental flows acted as homogeneous non-Newtonian fluids. Postyield behavior was typically shear thinning for clay-poor flows typical of the Italian field site (n = 0.4–0.7), while the clay-rich experiments exhibited near-Bingham characteristics. Most interesting is that most of these experiments had sand contents well in excess (>50%) of previously proposed limits for macroviscous behavior at strain rates relevant to debris-flow runout in channels and on fan surfaces (20%; Major and Pierson 1992). The fluid-like behavior we observed is a result of the relatively high viscosity of the interstitial fluids (silt and clay slurries) and the concentration of shear into narrow bands that helps sustain high shear rates during debris-flow runout.

Discussion

Transition to Frictional Behavior: Snout Dynamics. Many of the flows exhibited a thick snout near the front of the flow. As discussed above, only above a threshold body friction number ($N_{fl} > 100$) did the onset of frictional behavior in the snout become pronounced and significantly influence flow runout. We noticed from the first experiments that these frictionally locked snouts appeared drier and tended to have a greater portion of the largest clasts. This result was similar to the observations seen in the field by Genevois et al. (1999) and many other researchers (Suwa 1988; Iverson 1997*a*, 1997*b*, to name only a few). It is clear, however, that the lower fluid pressures documented in the snouts of fines-poor experimental debris flows by Iverson (1997*b*)—and used to explain snout formation in that case—cannot explain the frictional behavior of the snouts in our experimental flows. The conveyor-belt motion at the flow front preceding frictional lock-up guarantees that pore fluids reach the snout with the elevated pore pressures associated with the rapidly shearing and liquefied body of the flows. Given the silt and clay contents of our flows, elevated pore fluid pressures will only dissipate over timescales several orders of magnitude greater that the duration of the experiments (Major 2000). Some other mechanism(s) must be responsible for the onset of frictional behavior in our experiments.

These early observations prompted an experiment (experiment 10) where a snout was allowed to form and to arrest the flow. The deposit was sampled immediately following deposition for both water content and grain-size distribution. The results are shown along with the deposit depth profile (fig. 11). The water content dropped by nearly a half of a percent (error 0.1%), while the coarsest material increased systematically (error 0.3%) toward the leading edge of the snout. These measurements are not entirely independent. The addition of coarse material will increase the contribution of solids, decreasing the water content. Regardless, experiment 10 agreed with earlier, less systematic measurements that indicated that the water content dropped almost a percentage point in a similar flow.

Table 6. Rheologic Parameters if Bingham Behavior ($n = 1$) Is Assumed

Experiment (mix)	τ_o (Pa)	μ (Pa-s)	$URMS_{R_{cr}}$	$URMS_{U_p}$	$URMS_Q$
1 (fine)	98	1.92	12	6.6	.8
2 (medium fine)	80	1.48	1.8	.6	1.8
3 (medium coarse)	90	1.75	6.9	1.4	2
5 (medium)	14	.99	7.3	.7	.5
6 (medium coarse + 2% added clay)	124	.71	23	21	3.6
7 (medium coarse + 3% added clay)	68	1.5	.8	1.2	1.1
8 (fine)	77	4.1	8.4	7.1	3.7

Note. Uncertainties were calculated as in table 4.

There are undoubtedly many effects that a drier, coarser snout will have on the dimensionless parameters regulating the flow. However, the effects to the friction number N_f are most important to our particular flow regime. It can be seen in the formulation of N_f that the only way these two variables directly affect the value is through the volume of solids v_s. It will also indirectly affect the viscosity and the interstitial fluid density. However, both the lower water content and coarser material will raise the volume of solids, raising N_f by a factor of $v_s/(1 - v_s)$, a nonlinear quantity. With the increase of N_f, enhanced frictional interactions will decelerate the flow, decreasing shear, and further increasing N_f. Because water contents are small already (sometimes <15%), this positive feedback should be strong. Final locking of the flow also will be enhanced by the yield strength of the matrix because as the flow decelerates, local (grain-scale) shear stresses may drop below the matrix yield strength. During this entire process, the fluid behind the head should behave normally, experiencing a lower friction number. Flow in this region will ultimately back up behind the slower front and push the frictionally locked snout ahead as a moving dam that translates by boundary slip and occasionally by failure along discreet planes (fig. 4). Figure 12 is a schematic that describes this process.

Traditional theories describing snout development (e.g., Bagnold 1968; Takahashi 1980) have relied on granular effects to generate sorting of the largest clasts. Kinetic sieving and/or dispersive pressure are thought to float large clasts to the flow surface where velocities are largest so that these clasts are rapidly carried to the snout. In our extremely low Savage-number experiments, however, dispersive pressure will be negligible. Other work (Suwa 1988) has questioned the kinetic-sieving paradigm by insisting that the momentum of the largest particles carries them to the front of debris flows as the slope decreases. Though this mechanism is not appropriate to our constant flows, it does point out the possible importance of dynamic processes. Savage (1989) has pointed out that the kinetic sieving effect will have the further influence of trapping coarser particles at the snout while finer particles will be recirculated back into the body of the debris flow. In addition to this effect, a similar "fines-stripping" process may have contributed to the segregation of drier, coarser material into the snouts of our experimental flows: the fine-grained matrix slurry tends to be preferentially trapped in the dry, rough bed of the flume. This process may effectively strip fines and water from the snout region. A similar process has been observed in the field at the Jiang-Jia gully in China (Li et al. 1983).

Before further discussing the mechanisms by which coarse grains may be concentrated at the front of our experimental flows, it is first important to assess whether dynamic processes are indeed responsible. Because settling and stratification in the source tank could have had the effect of imposing a drier, coarser snout at the inflow, we performed an experiment to address this possibility specifically. To estimate the effect of settling in the supply tank, experiment 10 was performed to assess whether a snout would form after the material in the bottom half of the supply tank has run out (in the other channel). We sampled the material from the bottom half of the supply tank for grain size and water content during runout directly at the outflow. Four samples were obtained, including the initial release of material from the very bottom of the supply tank. The four samples obtained indicated variations of 0.1% in water content and 0.3% in the percentage of material coarser than 1 mm. We attributed these nonsystematic variations to measurement error. Recent work (Major 2000) has confirmed that settling is slow to occur in poorly sorted debris flows, particularly with the relatively high silt and clay contents of our debris mixtures. In an exhaustive series of experiments, Major (2000) found that elevated pore pressures in poorly sorted slurries remained high for tens of minutes. More-

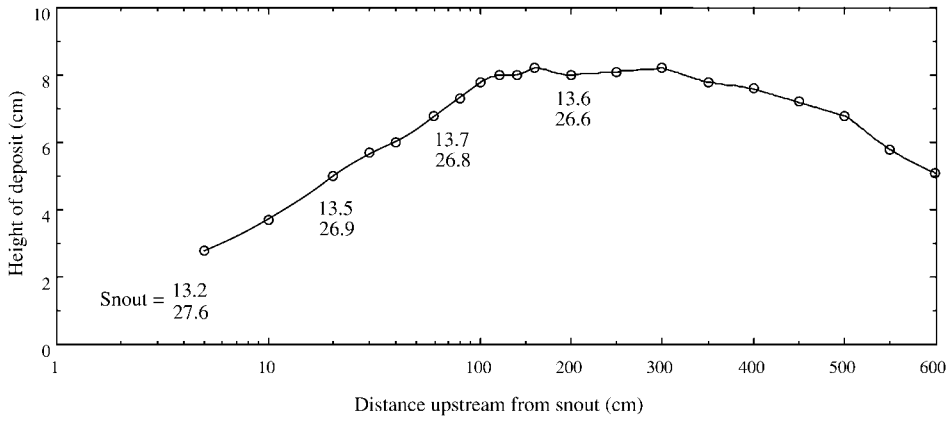

Figure 11. Depth profile of snout-arrested flow (experiment 11). The first number indicates the water content (in percent) obtained, while the second number indicates the percent (by mass) of material greater than a millimeter in diameter. Numbers are placed where each sample was obtained. Snout values were obtained at the tip of flow (i.e., distance upstream equals 0).

over, even with all of the debris from the lower half of the supply tank removed and sampled, we found a vigorous snout effect, as strong as any previous experiment (note that the data presented in fig. 10 comes from this experiment). Therefore, it would appear that the sorting and drying observed in figure 10 is indeed the result of some sort of dynamic process.

As mentioned above, stripping of fines from the leading edge of the flow and sequestering them in the dry, rough bed of the flume may have contributed to snout development. In fact, a rough calculation indicates that if dry walls were completely covered with matrix (to a depth of the wall roughness, 1 mm), all of the fine material and water could be removed from the snout in the first few meters of the channel, regardless of slurry composition. Therefore, two different experiments (5 and 9) were performed to investigate this effect. In these experiments, a given debris mixture was run down the same channel twice: once when the channel was dry, next when it was covered with a several mm thick layer of debris flow material (left over from the first run). In experiment 5 (medium grain-size distribution and moderate to strong snout development), snout speeds were slowed (see table 1) by 10%–20% when the channel boundary was dry, but there was no change in either the shape of velocity profiles observed in the body of the flow or the plug speed. Even though the "snout effect" was not enough to arrest the flow front in experiment 5, stripping of fines and water as the flow traverses a dry boundary does appear to enhance snout development.

A second experiment using a very coarse-grained mixture that developed a pronounced frictional snout that arrested the flow in the upper part of the channel (experiment 9), was influenced only slightly by the change in boundary condition. The first flow, which was run out over a dry bed, was arrested after only 0.9 m, while the second run, which flowed over an entirely mud-covered bed, ran out 1.3 m. Unfortunately, these flows advanced too short a distance down the flume to allow us to compare snout speeds. In addition, most of the difference in runout distance was likely controlled by the placement of support brackets along the channel. The support brackets only impede overbank flow. With very pronounced snout development, this blockage of overbanking flow sometimes caused flows to become arrested by effectively causing a sudden increase in volume of the frictionally locked part of the flow as the snout passed under the support bracket. Experiment 9A with the dry bed did not make it through the first support bracket at 0.9 m down flume. Experiment 9B with the wet bed made it through the first bracket but not the second. Therefore, it is difficult to even qualitatively assess the effect of the dry bed on this coarse-grained flow.

Regardless of the mechanism, sorting and local frictional interlocking of the snout region commonly occurred in flows where the body of the flow exhibited macroviscous, fluid-rheology behavior. In

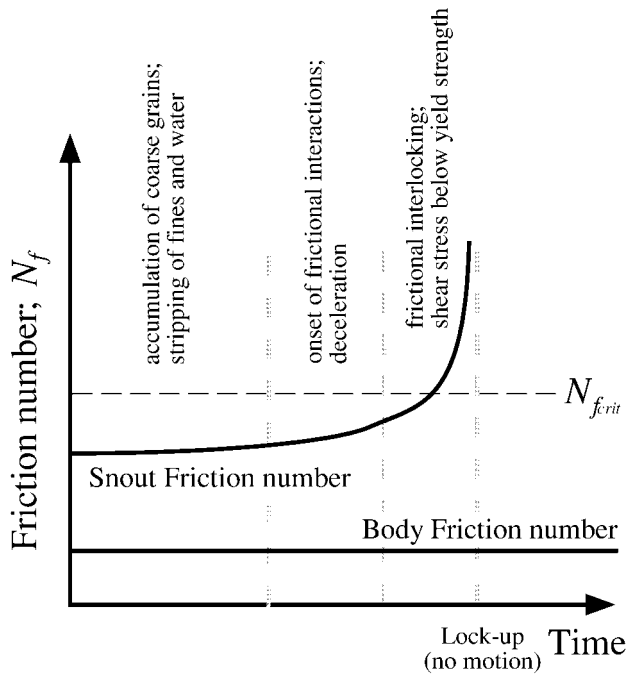

Figure 12. Schematic of the relative friction numbers as time progress in a snout-affected flow. The diagram illustrates the hypothetical path that the two friction numbers (body and snout) will proceed through with time. Notes illustrate hypothetical physical processes occurring at various times.

natural flows, the dams formed in this parameter regime (transitional between viscous and frictional) may often be pushed aside or bypassed as the bulk of the debris flows overbank (e.g., Suwa and Okuda 1983; Whipple and Dunne 1992; Whipple 1994). An interesting question, then, is whether and how fast a frictional snout is again formed by either kinetic-sieving or fluid-mechanical sorting. Additional experiments were performed where the snout was physically removed (by hand) from the channel during runout. The results indicated that the snout reformed quite rapidly (within a few meters), further supporting our interpretation that snout formation is a dynamic process. Figure 13 schematically illustrates the process described above and how it would extend to previous field observations (Whipple 1994). The deposits of such flows would have strong frictional signatures; however, the relative roles of frictional snout dynamics and fluid rheology in controlling flow runout and deposition rates and patterns are not yet clear.

Scale Effects and Experimental Limitations. The experimental facility used is considerably smaller than field-scale debris flows and some laboratory experiments (Iverson and LaHusen 1993; Iverson 1997*b*; Major 1997). The variables we measured and analyzed are by no means scale independent. For example, the yield strengths we report are more than enough to control dynamics in our flume but make up only a small (<1%) percentage of the resistance in flow depths similar to Berti et al. (1999). The grain-size distribution has also been truncated to only material smaller than 5 mm. In addition,

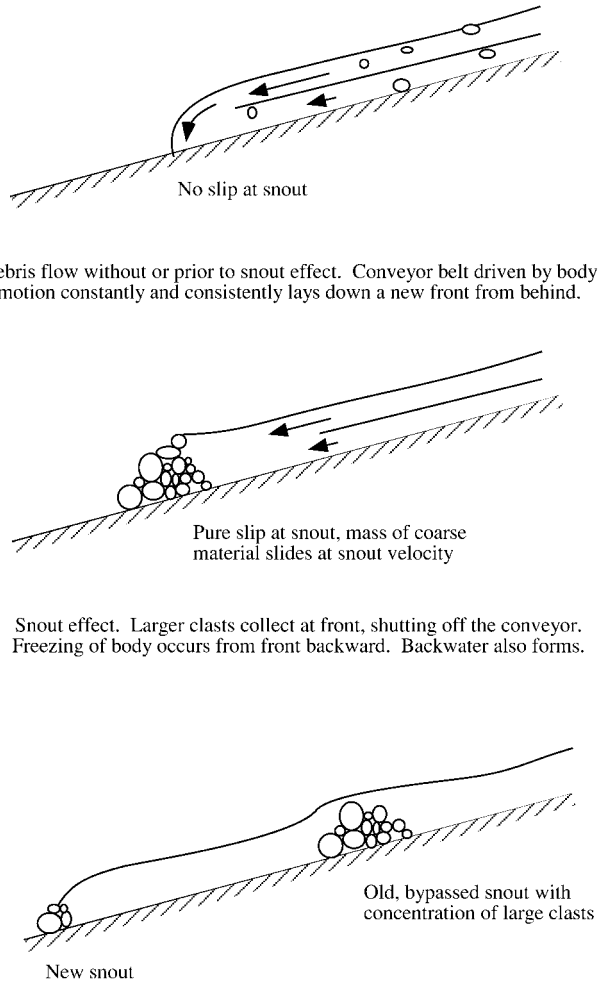

Figure 13. Schematic of the process hypothesized to occur in a frictional-snout, yield-strength-body debris flow. The final stage illustrates a series of clast piles, typical of those found by Whipple and Dunne (1992) and Whipple (1994).

experimental flow depths are about an order of magnitude less than typical debris flow depths. In short, many of the measured parameters cannot be directly related to field-scale flows.

However, the dimensionless variables and the conclusions based upon them are relevant to the physics of natural flows. The transition we describe should occur at roughly the same friction number in natural environments, when similar dimensionless representations are compared. Concentration of shear within narrow bands along channel banks can be seen in the observations of Berti et al. (1999). These higher shear rates will impact the rheology of the resisting layer (i.e., the material within the shear width). In fact, friction numbers in the lower reaches of Acquabona channel were approximately 300, very near the transition point investigated herein. Finally, the high interstitial viscosities reported herein will also be present in many natural flows, as natural debris flows commonly contain at least 10%–15% silt and clay by dry weight. Indeed, the viscosity relevant to the macroscopic friction number could be larger than the "matrix" viscosity used here, depending on the contribution of sand to the viscosity. Though these effects will not be important to all debris flows, many will be affected. In such flows, runout will be in part regulated by fluid rheology, even though they may exhibit some characteristics of granular behavior (e.g., a granular snout). Fast storm-induced flows that run through clayey or silty reaches (e.g., Berti et al. 1999), nonhydroplaning submarine debris flows, and fines-dominated lahars are just a few examples.

Summary and Conclusions

The transition from fluid-mud to grain-flow behavior is quite complicated and occurred at considerably lower friction numbers than expected from previous experimental constraints (Iverson 1997*b*). Frictional interactions were observed to occur at the snout of flows when body friction numbers were as low as 100. Despite the frictional interactions at the front, the bodies of all experiments remained fluid and can be best described by a non-Newtonian (shear thinning) fluid rheology including a finite, constant yield strength. Analysis suggested that the in situ rheology of our mixtures was moderately shear-thinning ($0.4 < n < 0.7$). With increases in clay and sand content, rheology tended to be more Bingham-like (n approximately unity). Effects of clay addition were particularly pronounced.

The relevant shear rates in all our experiments exceeded 5 s^{-1}, and most surpassed 20 s^{-1}, even though our slopes were relatively mild (10°–15°). Hypotheses set forth by earlier work (O'Brien and Julien 1988; Phillips and Davies 1991; Iverson 1997*b*) have suggested that shear rates greater than 5–10 s^{-1} are unusual and irrelevant. These conclusions, however, were based on the assumption that shear is distributed evenly throughout the flow. Shear concentrated considerably at the flow margins in all our experiments. Low shear rates (<5 s^{-1}) did occur locally in the snout and the nondeforming plug. In some cases (beyond a roughly defined critical body friction number of 100), these low shear rates and a suite of dynamic sorting and stripping mechanisms together caused frictional interlocking of the flow front. In a few experiments with the coarser debris mixtures, the damming effect of these frictional snouts caused the entire flow to arrest in the flume but only after the frictional snout was pushed a considerable distance by the fluid pressure building from upstream.

The in situ rheological results agree with earlier studies (Major and Pierson 1992; Coussot and Piau 1995), that observed shear-thinning or Bingham fluid behavior of natural debris flow mixtures (without a significant gravel component) for shear rates greater than 5 s^{-1}. Phillips and Davies (1991) and Major and Pierson (1992), however, reported very high instantaneous shear stresses in sand- and gravel-rich slurries, which they attributed to transient formation of clusters and chains of granular material. This onset of frictional behavior was taken to indicate a breakdown of the fluid rheology assumption at the strain rates relevant to debris flow runout in hazard zones for flows with greater than 20% sand. However, we observed fluid rheological behavior in free-surface flows with sand contents in excess of 50% (by volume) under flow conditions relevant to debris-flow runout. In part, this is because shear concentration in narrow bands sustained high shear rates in all of our experiments. In addition, it is possible that free-surface flows are less sensitive to the formation of transient grain clusters and chains because these granular clusters are much less likely to become trapped between solid boundaries than they are in co-axial or cone-and-plate viscometers.

The transition to frictional behavior in our free-surface experiments occurred only at the flow front where lower shear rates and a suite of dynamic sorting and stripping mechanisms together caused the frictional interlocking of the flow front. Settling and stratification in the supply tank were definitively ruled out as potential causes of the coarser and drier snouts. Further, we have demonstrated that dynamic sorting mechanisms (e.g., kinetic

sieving) acting alone were not sufficient to trigger the rapid formation and re-formation of frictional snouts. We postulate that the dynamic concentration of coarser material at the flow front increases the local friction number, thus inhibiting internal deformation and triggering a series of positive feedbacks that quickly result in a wholesale frictional interlocking of the snout region. Despite limitations of the experimental set up in regards to the maximum size of clasts and the magnitude of normal stresses developed in shallow experimental flows, we anticipate that the macroviscous to frictional transition in field-scale debris flows probably occurs via a similar suite of mechanisms and ought to occur at approximately the same friction number. In our view the greatest obstacle to translation of experimental results to field scale lies in determining the appropriate values of the representative grain size δ and the "fluid" viscosity μ in the non-dimensional scaling numbers used to gauge flow regime.

ACKNOWLEDGMENTS

This research was financially supported by MIT and Chevron. A. Simoni's stay at MIT was kindly sponsored by CNR-GNDCI (National Research Council of Italy) within the CNR-MIT Cooperation on Climate Change and Hydrogeological Disasters in the Mediterranean Area program. We thank G. Parker and D. Mohrig for helping develop the experimental technique and J. Southard for his advice and donating the shell of the flume for the experiments. Also thanks to S. DiBenedetto, N. Snyder, B. Lyons, and M. Hendricks for their assistance in performing the experiments and C. Mei for the use of his viscometer. The manuscript benefited from careful reviews by P. Coussot, L. Pratson, and two anonymous reviewers.

REFERENCES CITED

Bagnold, R. A. 1954. Experiments on a gravity-free dispersion of large solid spheres in a Newtonian fluid under shear. Proc. R. Soc. Lond. 225:49–63.

———. 1968. Deposition in the process of hydraulic transport. Sedimentology 10:45–56.

Berti, M.; Genevois, R.; Simoni, A.; and Tecca, P. R. 1999. Field observation of a debris flow event in the Dolomites. Geomorphology 29:265–274.

Costa, J. E. 1984. Physical geomorphology of debris flows. *In* Costa, J. E., and Fleisher, P. J., eds. Developments and applications of geomorphology. Berlin, Springer, p. 268–317.

Coussot, P. 1994. Steady, laminar flow of concentrated mud suspensions in open channel. J. Hydrol. Res. 32: 535–559.

Coussot, P., and Meunier, M. 1996. Recognition, classification and mechanical description of debris flows. Earth Sci. Rev. 40:209–227.

Coussot, P., and Piau, J. 1995. A large-scale field coaxial cylinder rheometer for the study of the rheology of natural coarse suspensions. J. Rheol. 39:105–124.

Fairchild, L. H. 1985. Lahars at Mt. St. Helens. Unpub. Ph.D. dissertation, University of Washington, Seattle.

Genevois, R.; Berti, M.; Ghirotti, M.; Simoni, A.; and Tecca, P. R. 1999. Debris flow monitoring and analysis in the Dolomitic Region (Upper Boite Valley, Italian Alps). Thematic report, EC project, ENV4.CT96.0253 (Vol. 2), Brussels, 58 p.

Haff, P. K. 1986. A physical picture of kinetic granular fluids. J. Rheol. 30:931–948.

Huang, X., and García, M. H. 1999. Modeling of non-hydroplaning mudflows on continental slopes. Mar. Geol. 154:131–142.

Iverson, R. M. 1997*a*. Hydraulic modeling of unsteady debris-flow surges with solid-fluid interactions. *In* Debris-flow hazards mitigation: mechanics, prediction and assessment. Proceedings of the First International Conference Water Resources Engineering Division/American Society of Civil Engineers (San Francisco, August 7–9), New York, American Society of Civil Engineers, p. 550–560.

———. 1997*b*. The physics of debris flows. Rev. Geophys. 35:245–296.

Iverson, R. M., and LaHusen, R. G. 1993. Friction in debris flows: inferences from large-scale flume experiments. *In* Shen, H. W.; Su, S. T.; and Wen, F., eds. Hydraulic engineering 1993. Proceedings of the 1993 Conference (San Francisco, July 25–30). New York, American Society of Civil Engineers, p. 1604–1609.

Johnson, A. M. 1965. A model for debris flow. Unpub. Ph.D. dissertation. Pennsylvania State University, University Park.

———. 1970. Physical processes in geology. San Francisco, Freeman, Cooper, 577 p.

Kang, Z., and Zhang, S. 1980. A preliminary analysis of of the characteristics of debris flow. *In* Proceedings of the International Symposium on River Sedimentation, Beijing, Chinese Society for Hydraulic Engineering, p. 225–226.

Li, J.; Yuan, J.; Bi, C.; and Luo, D. 1983. The main features of the mudflow in Jiang-Jia Ravine. Z. Geomorphol. 27:325–341.

Major, J. J. 1997. Depositional processes in large-scale debris-flow experiments. J. Geol. 105:345–366.

———. 2000. Gravity-driven consolidation of granular

slurries—implications for debris-flow deposition and deposit characteristics. J. Sediment. Res. 70:64–83.
Major, J. J., and Pierson, T. C. 1992. Debris flow rheology: experimental analysis of fine-grained slurries. Water Resour. Res. 28:841–857.
Mohrig, D.; Elverhoi, A.; and Parker, G. 1999. Experiments on the relative mobility of muddy subaqueous and subaerial debris flows, and their capacity to remobilize antecedent deposits. Mar. Geol. 154:117–129.
Mohrig, D.; Whipple, K. X.; Hondzo, M.; Ellis, C.; and Parker, G. 1998. Hydroplaning of subaqueous debris flows. Geol. Soc. Am. Bull. 110:387–394.
O'Brien, J. S., and Julien, P. Y. 1988, Laboratory analysis of mudflow properties. J. Hydrol. Eng. 114:877–887.
Phillips, C. J., and Davies, T. R. H. 1991. Determining rheological parameters of debris flow material. Geomorphology 4:101–110.
Savage, S. B. 1984. The mechanics of rapid granular flows. Adv. Appl. Mech. 24:289–366.
———. 1989. Flow of granular materials. *In* Germain, P.; Piau, M.; and Caillerie, D. Theoretical and applied mechanics. Amsterdam, Elsevier, p. 241–266.
Savage, S. B., and Hutter, K. 1989 The motion of a finite mass of granular material down a rough incline. J. Fluid Mech. 199:177–215.
Schmeeckle, M. 1992. Rheological measurements of highly concentrated silt-water mixtures using a recirculating mud flume. M.S. thesis, University of Washington, Seattle.
Schwab, W. C.; Lee, H. J.; Twichell, D. C.; Locat, J.; Nelson, C. H.; McArthur, W. G.; and Kenyon, N. H. 1996. Sediment mass-flow processes on a depositional lobe, outer Mississippi fan. J. Sed. Res. 66:916–927.
Simoni, A. 1998. Innesco e mobilizzazione di debris flow: il bacino sperimentale di Acquabona. Ph.D. thesis, Universita di Bologna.
Suwa, H. 1988. Focusing mechanism of large boulders to a debris-flow front. Trans. Jpn. Geomorphol. Union 9: 151–178.
Suwa, H., and Okuda, S. 1983. Deposition of debris flows on a fan surface, Mt. Yakedake, Japan. Z. Geomorphol. Suppl. 46:79–101.
Takahashi, T. 1980. Debris flow in prismatic open channel. J. Hydrol. Eng. 106:381–396.
———. 1981. Debris flow. Annu. Rev. Fluid Mech. 13: 57–77.
Thomas, D. G. 1965. Transport characteristics of suspension. VII. A note on the viscosity of Newtonian suspensions of uniform spherical particles. J. Colloid Sci. 20:267–277.
Whipple, K. X. 1994. Debris flow fans: process and form. Ph.D. thesis, University of Washington.
———. 1997. Open-channel flow of Bingham fluids: applications in debris-flow research. J. Geol. 105:243–262.
Whipple, K. X., and Dunne, T. 1992. The influence of debris-flow rheology on fan morphology, Owens Valley, California. Geol. Soc. Am. Bull. 104:887–900.
Yano, K., and Daido, A. 1965. Fundamental study on mudflow. Bull. Disaster Prev. Res. Inst. 14:69–83.